# MRAS Observer Based on Rotor Current for DFIG Sensorless Control inNetwork Voltage Drop Condition

Ali. Khodadadi, Mohammad Esmaeil.Akbari,Mohsen.Ebadpour, Hosein.NasirAghdam
Department of Electrical Engineering, Ahar Branch, Islamic Azad University, Ahar, Iran
Email: alikhodadadi1992@gmail.com (Corresponding Author)
Email:m.akbari@tptco.net

## Abstract

*This paper introduces a new application of the Rotor based-current MRAS observer (RCMO) method for Doubly fed induction generator (DFIG) sensorless control in the condition of network voltage drop. DFIG control is Field oriented control (FOC) vector and Model reference adaptive system (MRAS) observer is used instead of speed and position sensor based on rotor current. It is possible to estimate the speed and position of the rotor. Simulation and analysis have been done based on 10% balanced voltage drop in the wind power plant terminal. The results of the simulation show the estimated speed ($\hat{\omega_r}$), accurate and appropriate sequence of speed has real ($\omega_r$). Also, the graph of the machine variables in the state of balanced three-phase voltage drop in the state sensored is obtained and compared with the state sensorless, which shows the lack of influence of the estimated speed fault on the simulation results and the acceptability of using the RCMO method in estimating the speed in the condition of balanced voltage drop. Finally, the effect of various voltage drops on the estimated speed fault has been investigated.*

**Keywords:** Vector control, Sensorless, DFIG, RCMO.

## 1. Introduction

Wind power generation has increased in recent years. Types of generators wind power plants include: induction (included: Squirrel cage induction and double feeding induction) and synchronous (included: Permanent magnet synchronous and rotor excitation synchronous) [1]. DFIG generator due to many advantages have made it the most widely used wind generator. Its advantages can be to flexibility (variable speed with frequency constant exploitation), smaller converter (About 30% generator power), being resistant to changing parameters, four-zone PQ, lower price and losses
Pointed out below. But despite the great penetration of DFIG in electrical networks, many problems still exist: Including the stability and quality of network power, ability to overcome voltage drop and short circuit and phase imbalance, operation sensorsless and MPPT (Maximum power point tracking). The DFIG control system needs rotor speed and rotor position parameters. In sensored methods, the speed and position of the rotor are measured with a sensor and applied to the control system [2][3]. Position and speed sensors have disadvantage including : need to repair and Maintenance, expensive, the vulnerability of the communication cable between the sensor and the control system [4], therefore, vector control sensorless has become popular. Articles related to there are three types of sensorless control methods [18]: a) open loop sensorless methods b) methods based on MRAS c) other sensorless methods (such as PLL). Articles [5-6] with open loop sensorless method, the rotor position is determined by comparing the estimated rotor current with its measured current. Open loop method based on current estimation only the rotor is not built, but it is suggested in the observational article [10]

based on $i_m$. Also, in the article [11], an observation based on the rotor flux is proposed. The disadvantage of this method: The rotation speed is obtained from the derivative of the estimated $\theta_{slip}$, Therefore high frequency noise can be amplified. Also, in the article [11], an observation based on the rotor flux is proposed. The article [12] is the first article that proposed the MRAS method for sensorless control of the squirrel cage induction machine. In this paper, the observer design is discussed and a small signal model is also proposed. [13-14] it is the first paper to apply MRAS to DFIG sensorless controller, but about dynamics observer, control design process, precision sensorless and and sensitivity to change machine parameters, mention did not bring. In [16], the estimated variable is the stator flux. In this article, the small signal model, sensitivity to change machine parameters and also the design process of an MRAS observer, has been presented. In this article, the required magnetic current is completely provided by the network. Therefore the observer can not follow the rotational speed. In [11-13], an MRAS observer based on rotor current (RCMO) is proposed that both for island mode and for Network connected mode is applicable. The advantage of RCMO over other MRAS observers is that this observer can used to DFIG control, even if be connected to the network. That is, since magnetizing current entirely from the stator is provided, if $i_{dro}$ = 0, because $i_{r0}$ is opposite to zero, then the system will not become unstable. Another advantage of RCMO is to synchronize DFIG is compatible with the network. In [11-13] a MRAS observer based on rotor current (RCMO) is proposed for both islanded and network dependent mode is applicable. The advantage of RCMO over other MRAS observers is that this observer can even if it is used to control DFIG, connect to the network. That is, since magnetizing current completely from the stator is provided if $i_{dro}$ = 0, because $i_{r0}$ is opposite to zero, then the system will not become unstable. Another advantage of RCMO is its suitability for synchronizing the DFIG with the network. [11-15] have proposed a new method of MRAS that obtains $i_r$ with a moment-based MRAS observer (TBMO). In [20-21] PLL sensorless control it has been suggested, but the test has not been implemented. According to the result of the article [22] the most acceptable the sensorless control method for DFIG is the RCMO scheme, which provides a suitable response from DFIG provides. In more methodical articles sensorless the RCMO, it is used in normal working mode, that is, in the mode without voltage drop of the network connected to the DFIG, check and similar have made; Therefore, in this article, the sensorless control of DFIG with RCMO in the condition of three-phase voltage drop in the network is discussed. This article in five the section is set: in the second section, the DFIG model and vector control are explained. In the third part, the proposed method in estimation the speed and position of the rotor are described. In the fourth part, simulation and its results is provided. The fifth section presents the conclusion.

## 2. DFIG Model and itsVector Control

A grid-connected DFIG wind farm is shown in Figure 1. Wind mechanical power ($P_{mec}$) from the axis side is transferred to DFIG. The effective factors in the amount of electrical energy produced in DFIG are: Wind speed, coefficient turbine aerodynamics, and operating point DFIG. The two-way power ($P_r$) enters (or leaves) the rotor circuit after passing through the back-to-back converters. These two converters it consists of: rotor side converter (RSC) whose task is to control DFIG power and stator side converter (GSC) whose task is to adjust DC link voltage and power factor control the point is PCC. The equations of the machine based on the $d_q$ reference frame rotating with synchronous speed are:

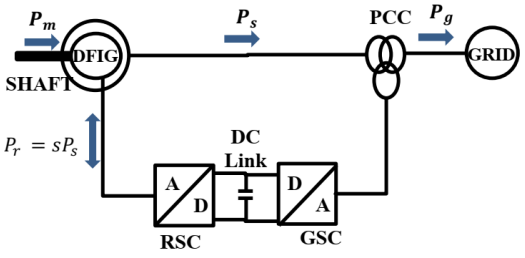


**Fig. 1.** DFIG grid connected wind farm.

$$V_{ds} = R_s i_{ds} + \frac{d\lambda_{ds}}{dt} - \omega_e \lambda_{qs} \quad (1)$$

$$V_{qs} = R_s i_{qs} + \frac{d\lambda_{qs}}{dt} - \omega_e \lambda_{qs} \quad (2)$$

$$V_{dr} = R_r i_{dr} + \frac{d\lambda_{dr}}{dt} - (\omega_e - \omega_r)\lambda_{qr} \quad (3)$$

$$V_{qr} = R_r i_{qr} + \frac{d\lambda_{qr}}{dt} - (\omega_e - \omega_r)\lambda_{dr} \quad (4)$$

$$\lambda_{ds} = L_s i_{ds} + L_m i_{dr} = L_m i_{ms} \quad (5)$$

$$\lambda_{qs} = L_s i_{qs} + L_m i_{qr} \quad (6)$$

$$\lambda_{dr} = L_m i_{ds} + L_r i_{dr} \quad (7)$$

$$\lambda_{ir} = L_m i_{qs} + L_r i_{qr} \quad (8)$$

$$T_e = 3\frac{p}{2} L_m (i_{qs} i_{dr} - i_{ds} i_{qr}) \quad (9)$$

With the reference assumption about the stator flux vector, we have: $\lambda_{qs} = 0$ from (5) we have:

$$i_{ms} = \frac{\lambda_{ds}}{L_m} \quad (10)$$

and from (6) we have:

$$i_{qr} = \frac{-L_s}{L_m} i_{qs} \quad (11)$$

assuming constant stator flux in equation (1) it becomes as follows:

$$\begin{cases} v_{ds} = R_s i_{ds} \\ v_{qs} = R_s i_{qs} + \omega_e \lambda_{ds} \end{cases} \quad (12)$$

From formula (10) and (11) according to if $\lambda_{qs} = 0$, the following equation is obtained:

$$\tau_{ms} \frac{di_{ms}}{dt} + i_{ms} = i_{dr} + \frac{1-\sigma_s}{R_s} v_{ds} \quad (13)$$

$$T_e = -3\frac{p}{2}\frac{L_m^2}{L_s} i_{ms} i_{qr} \quad (14)$$

In (12), $v_{ds}$ seems small, therefore, we conclude from equation (13) that $i_{ms}$ can be controlled by $i_{dr}$, and from equation (11) $i_{qr}$ can also be controlled by $i_{qs}$ controlled.

$$i^*_{qr} = -\frac{L_s}{L_m} i_{qs} \quad (15)$$

according to equation (12) $i_{ms}$ and $i_{qr}$ in $T_e$ are effective For voltage demodulation $\theta_{slip}$ rotor is used.

$$\theta_{slip} = \theta_e - \hat{\theta}_r = \int \omega^*_e dt - \hat{\theta}_r \quad (16)$$

$\theta_e$ is obtained from the following equation:

$$\theta_e = \tan^{-1}(\lambda_{\beta s} / \lambda_{\alpha s}) \quad (17)$$

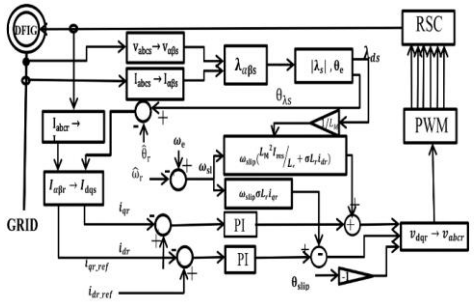


**Fig. 2.** DFIG sensorless control.

The component αβ related to $\lambda_s$ is obtained from the stator voltages and currents.

$$\begin{cases} \lambda_{\alpha s} = \int (v_{\alpha s} - R_s i_{\alpha s}) dt \\ \lambda_{\beta s} = \int (v_{\beta s} - R_s i_{\beta s}) dt \end{cases} \quad (18)$$

From the combination of equations (3), (4), (7) and (8) two the following equation is obtained:

$$V_{dr} = R_r i_{dr} + \sigma L_r s i_{dr} - \omega_{slip} \sigma L_r i_{qr} \quad (19)$$

$$V_{qr} = R_r i_{qr} + \sigma L_r s i_{qr} - \omega_{slip}\left(\frac{L_m^2 i_{ms}}{L_s} + \sigma L_r i_{dr}\right) \quad (20)$$

where σ in the above equations is: $\alpha = 1 - \frac{L_m^2}{(L_s L_r)}$ (21)

From equation (19) and (20) two equations

the following is obtained:

$$\frac{di_{dr}}{dt} = -\frac{R_r}{\sigma L_r} i_{dr} + \frac{1}{\sigma L_r} v_{dr} + \omega_{sl} i_{qr} \quad (22)$$

$$\frac{di_{qr}}{dt} = -\frac{R_r}{\sigma L_r} i_{qr} + \frac{1}{\sigma L_r} v_{qr} + \omega_{sl} i_{dr} + v_q \quad (23)$$

where $v_q$ is:

$$v_q = \frac{\omega_{sl} {L_m}^2 i_{ms}}{\sigma L_r L_s} \quad (24)$$

Figure 2 shows the proposed control system based on vector control (VC) method. In this figure, first the rotor current is measured ($i_{abcr}$) and is taken Then it is converted into $d_q$ components of the current ($i_{dqr}$) and then it is subtracted from the reference value ($i_{dqr\text{-}ref}$). The result is input to two PI controllers. to the output of PI controllers $\omega_{slip}(\frac{{L_m}^2 i_{ms}}{L_s} + \sigma L_r i_{dr})$ and also $-\omega_{slip}\sigma L_r i_{qr}$ it will be added; As a result, the orthogonal rotor voltages $v_{dqr}$ that must be applied to the rotor are obtained. These orthogonal voltages are converted to three-phase rotor voltage using park conversion and then applied to RSC. It should be noted that in this article only RSC is controlled and GSC control is omitted. In this flowchart, $\theta_e$ and $\theta_r$ angles are needed to convert park to $\theta_{slip}$ be obtained. To calculate $\theta_e$ first stator current and voltage are measured ($i_{abcs}$,$v_{ibcs}$), and then αβ components are obtained by Clark transformation. Using the equation (18), the stator magnetization ( $\lambda_{\alpha\beta s}$ ) is obtained. We use equation (17) to calculate $\theta_e$. Also, $\lambda_{ds}$ is needed to calculate ims in the expression $\omega_{slip}(\frac{{L_m}^2 i_{ms}}{L_s} + \sigma L_r i_{dr})$ according to equation (10); therefore we have:

$$\lambda_{ds} = \sqrt{{\lambda_{\alpha s}}^2 + {\lambda_{\beta s}}^2} \quad (25)$$

The reference currents are obtained with the help of equations (5), (6) and (12) as follows.

$$i_{dr-ref} = v_{qs} / (\omega_e L_m) \quad (26)$$

$$i_{qr-ref} = -2T_e L_s / (3P{L_m}^2 i_{dr-ref}) \quad (27)$$

$\hat{\omega}_r$ and $\hat{\theta}_r$ are shown in Figure 2, is obtained from RCMO, which will be explained in the next section.

## 3. Estimate the speed and position of the rotor with RCMO

In this article, a MARS observer who the base current of the rotor is established, the speed and estimates the position of the DFIG rotor. DFIG control is done with $\hat{\omega}r$ and $\hat{\theta}_r$. As discussed in articles [13, 11, and 21] the MARS observer is based on an adaptive model and a signal reference model. The reference model in this article is the measurement current $i_r$ and the adaptive model is the estimated current $\hat{i}_r$ which is obtained from $v_s$ and $i_s$. Figure 2 shows the block diagram of RCMO. In this figure, the adaptive model and the reference model are shown with dashed lines. Stator flux in static frame (s) consists of:

$$\lambda_s = L_s i_s + L_m i_r e^{j\theta_r} \quad (28)$$

The stator current can be obtained from the equation (19) obtained:

$$i_r = \frac{\lambda_s - L_s i_s}{L_m} e^{-j\hat{\theta}r} \quad (29)$$

By substituting $\hat{\theta}_r$ instead of $\theta_r$ in (20), the estimated rotor current is obtained:

$$\hat{i}_r = \frac{\lambda_s - L_s i_s}{L_m} e^{-j\hat{\theta}r} \quad (30)$$

The fault between the αβ components of the estimated current rotor ($\hat{i}_r$) and rotor measurement process ($i_r$), is defined by outside multiplication.

$$\xi = \hat{i}_{\alpha r} i_{\beta r} - \hat{i}_{\beta r} i_{\alpha r} = \left| i_r \right| \left| \hat{i}_r \right| \sin(\theta_{er}) \quad (31)$$

We get a correct estimate of $\theta_r$ when: $\theta_{er} = 0$.

In Figure 3, the RCMO estimator is shown. The output of this the estimator is $\theta_r$, which is used to modulate and demodulate the currents and voltages of the rotor. In this case, $i_{ms}$ can be supplied from the rotor or stator. $i_{dr}$ is used to inject Q into the network. $i_{qr}$ is also used to adjust active power injection according to equation (14). Measuring rotor current ($i_r$) with speed ($\omega_e - \omega_r$) and the estimated rotor current ($\hat{i}_r$) with the speed ($\omega_e - \hat{\omega_r}$) rotates, so $\hat{i}_r$ rotates with the speed ($\omega_r - \hat{\omega_r}$) relative to $i_r$. Regardless of the initial conditions, we have:

$$\theta_e = (\omega_r - \hat{\omega}_r)/s$$

Assuming that all machine parameters are correctly identified and introduced. At we have a working point:

$$i_{ro} = \hat{i}_{ro}, \theta_e = \theta_e = 0 \quad (32)$$

Therefore, by linearizing the equation (22), you will have:

$$\xi = |i_{ro}|^2 . \theta_e \Rightarrow \xi = |i_{ro}|^2 \frac{\omega_r - \hat{\omega}_r}{s} \quad (33)$$

In Figure 3 of the PI controller,

set the estimated rotor speed $\hat{\omega}_r$ and the error of the equation (22) reduces to zero. By changing power DFIG output, $|i_r|$ also changes, so there is a variable gain in the conversion function (24). To compensate for this, a variable gain of $|i_{ro}|^{-2}$ is used in the diagram block.

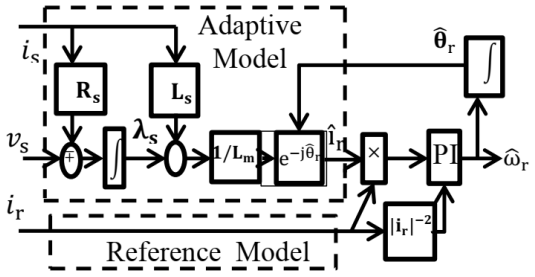


**Fig. 3.** RCMO block diagram.

## 4. Simulation results

In this section, we study the DFIG wind power plant connected to the grid for a constant load (1 KW active) in three modes and evaluate the correctness of the operation of the power plant set and control documents.

**a)** First, by creating disturbance of voltage drop balanced 10% at the connection point of the wind power plant to the grid (PCC), wind power plant parameters such as the voltage and current of the stator and rotor in two modes sensored and sensorsless are obtained and compared.

**b)** In the next step, we change the speed of the rotor according to a certain reference and then study and check the sequence on the estimated speed from the reference speed.

**c)** In the third step, by creating a balanced voltage drop disturbance (with different percentages) in the DFIG terminal, the amount of deviation of the estimated speed from the actual speed is studied and checked. Also, the values of DFIG parameters are according to Table 1.

**Table 1.** DFIG parameters.

| | |
|---|---|
| Nominal power: 2 MW | Stator resistance: 12.5 Ω |
| Nominal stator voltage: 380 V | Rotor resistance: 12.5 Ω |
| Nominal rotor voltage: 380 V | Stator inductance: 0.071 H |
| Nominal frequency: 50Hz | Rotor inductance: 0.071 H |
| Number of pairs pole: 2 | Magnetizing inductance: 0.0477 H |
| | Leakage inductance : 0.071 H |

**a)** In this case, we consider the sensor control system. We keep the rotor speed constant at 1750 rpm and create a 10% voltage drop in PCC in 1.8 to 2.2 seconds. We leave the load unchanged (1 KW active). Figure 2 shows the power output diagram of the power plant, stator voltage, and rotor and stator current. As seen in this figure, in the time interval of 1.8 seconds to 2.2 seconds, when 10% of the voltage is

created, the active power is reduced and the reactive power is increased. Also, the current amplitude of the stator rotor has decreased in the above time interval. Figure 6 also shows the power output of the power plant, stator voltage, and rotor and stator current in sensorless mode, in voltage drop mode 10% shows three balanced phases (within a time interval of 1.8 second to 2.2 second) in the terminal wind generator. As seen in Figure 6 the time interval from 1.8 seconds to 2.2 seconds, when the voltage drop is 10%, the active power is reduced and the reactive power is increased. Also, the current amplitude of the stator rotor has decreased in the above time interval. Also, the estimation speed drops in this time interval. From the comparison of the simulation curves in Figures 2 and 6, it can be concluded that all the curves are the same. And the speed estimation fault did not affect the graphs of DFIG variables.

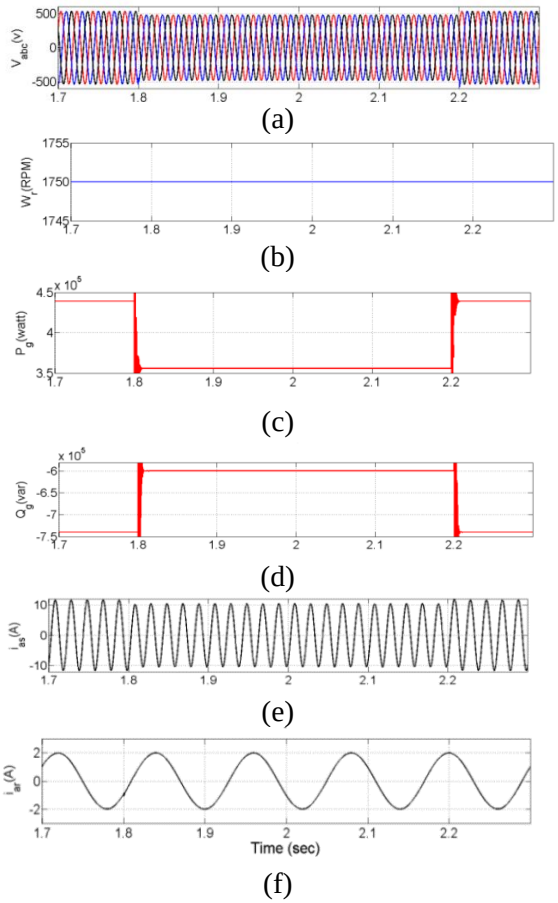


**Fig. 4.** The diagram of the variables of the machine in the three-phase voltage of the sensored at the moment [t= 1.8-2.2] seconds (a) three-phase stator voltage (b) speed rotor (c) output active power from (d) DFIG reactive power output from (e) The output stator a phase current from DFIG (f) DFIG phase current of a rotor related to DFIG.

**b)** In this case, the reference speed ($\omega_r$) has changed from 1350 rpm to 1750 rpm during 2.2 seconds. This increase in speed is equivalent to 400 rpm which occurred at a slope of 182 rpm per second. This speed increase rate is usually lower than the actual wind speed increase rate. Figure 3 compares the estimated speed ($\hat{\omega}r$) with the reference. Figure 3 shows that the estimated speed $\hat{\omega_r}$ closely follows the reference speed $\omega_r$. If the reference speed ($\omega_r$) decreases from 1750 rpm to 1350 rpm during the same period of 2.2 seconds (that is, with a decrease rate of 182 rpm in seconds and less than the actual deceleration rate wind), the estimated speed ($\hat{\omega_r}$) closely follows the reference speed ($\omega_r$). Figure 1. Comparison diagram of $\omega_r$ and $\hat{\omega_r}$ shows.

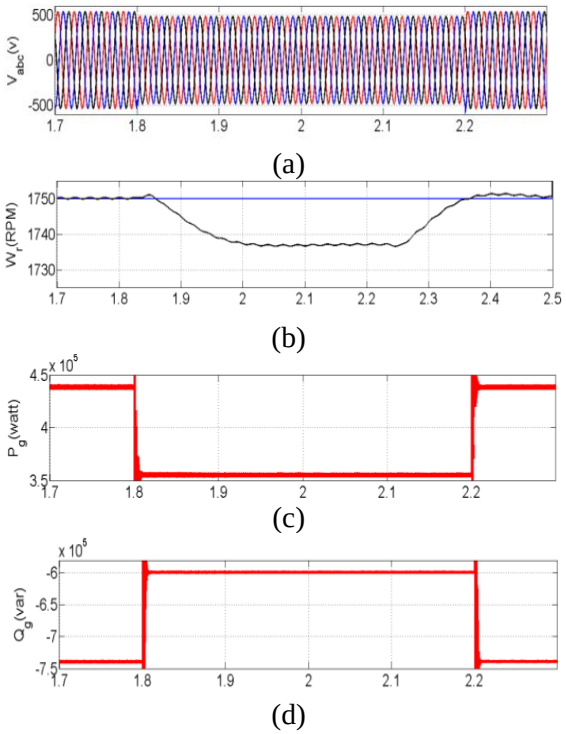

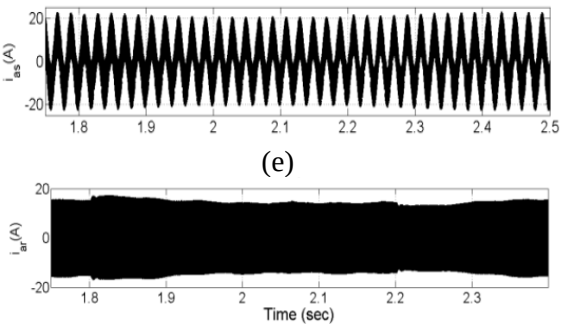


**Fig. 5.** The diagram of the variables of the machine in the three-phase voltage of the sensorless at the moment [t= 1.8-2.2] seconds (a) three-phase stator voltage (b) Estimated rotor speed (c) output active power from (d) DFIG reactive power output from (e) The output stator a phase current from DFIG (f) DFIG phase current of a rotor related to DFIG. As seen in Figure 1, speed reference (ωr) at the moment of 2.3 seconds from 1750 rpm to 1350 rpm has been reduced in 2.6 seconds. The estimated speed ($\hat{\omega_r}$) also followed $\omega_r$ with an acceptable fault.

**c)** In this case, different voltage drops applied in PCC. The estimated speed fault for each voltage drop is obtained from the simulation and is shown in Table 1.

**Table 1.** Estimated speed deviation.

| | | | | | |
|---|---|---|---|---|---|
| 20 | 15 | 10 | 5 | 0 | Voltage drop in PCC(%) |
| 29 | 20.5 | 13 | 6 | 0 | Estimated speed deviation (RMP) |
| 1.7 | 1.2 | 0.7 | 0.3 | 0 | Estimated speed deviation (%) |

As seen in Table 1, with the increase in voltage drop in PCC, the estimated speed deviation $\hat{\omega_r}$ also increases. From the article [13], it can be said that the deviation of the speed up to about 20 revolutions per minute is acceptable. Low voltage drop in power networks is usually maximum 5%. The estimated speed deviation in 6% voltage drop is 3 turns minutes; Therefore, RCMO output in voltage drop is low, suitable and desirable.

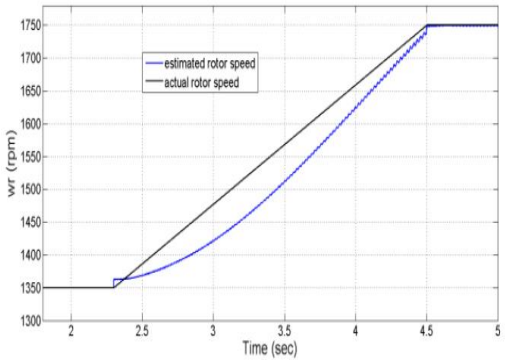


**Fig. 6.** Comparison chart $\omega_r$ and $\hat{\omega_r}$ during increasing speed.

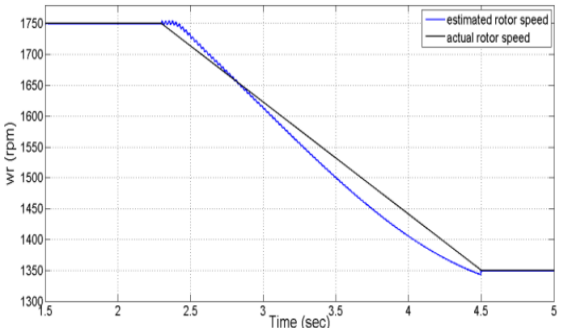


**Fig. 7.** Comparison chart $\omega_r$ and $\hat{\omega_r}$ during descreasing speed.

Table 2 shows values of $k_p$ and $k_I$ related to PIs controller and RCMO.

**Table 2.** Values $k_p$ and $k_I$.

| controller | $k_p$ | $k_I$ |
|---|---|---|
| PI($i_{dr}$) | 911 | 0.006 |
| PI($i_{qr}$) | 933 | 0.06 |
| PI(RCMO) | 111 | 0.06 |
| Integrator(RCMO) | ----- | 0.85 |

## Conclusion

This article introduces a new application of the RCMO method for sensorless control of DFIG connected to the network in the condition of network voltage drop. The DFIG control is vector (FOC) and instead of the speed (and position) sensor, the MRAS observer is used based on the rotor current to estimate the speed and position of the

rotor. Simulation and analysis for the balanced voltage drop in the terminal of the wind power plant has been done 10% voltage drop is considered. The simulation results show that the estimated speed ($\hat{\omega_r}$) accurate and appropriate tracking of speed has real ($\omega_r$). Also, the diagram of machine variables in the state of balanced three-phase voltage drop in the state sensored has been obtained and compared with the sensorless mode which indicates that the estimated speed fault does not affect the simulation results and the acceptability of RCMO method application in the condition of balanced voltage drop in the terminal of wind power plant. Finally, the effect of various voltage drops on the estimated speed fault has been investigated.

| | | | |
|---|---|---|---|
| Rotor inertia | $J$ | Magnetizing current | $i_{ms}$ |
| Stator resistance | $R_s$ | Stator current | $i_s$ |
| Rotor resistance | $R_r$ | Rotor current | $i_r$ |
| Synchronous angular frequency | $\omega_e$ | Stator inductance | $L_s$ |
| Rotor angular frequency | $\omega_r$ | Rotor inductance | $L_r$ |
| Slip angular frequency | $\omega_{sl}$ | Magnetizing inductance | $L_m$ |
| Rotor angular frequency-estimated | $\hat{\omega}_r$ | Leakage inductance | $L_l$ |
| Laplace operator | S | Stator flux | $\lambda_s$ |
| Number of pole pairs generator | P | Rotor flux | $\lambda_r$ |
| - | - | Electromagnetic torque | $T_e$ |

## Appendix a

## References


[1] J. -H. Lee, Y. -C. Kwon and S. -K. Sul, "HighFidelity Induction Motor Simulation Model Based on Finite Element Analysis," in IEEE Transactions on Industrial Electronics, vol. 69, no. 10, pp. 9872-9883, Oct. 2022.

[2] M. A. Asha Rani, C. Nagamani, G. Saravana Ilango, and A. Karthikeyan, "An Effective Reference Generation Scheme for DFIG With Unbalanced Grid Voltage" IEEE Trans. on Sustainable Energy, VOL. 5, NO. 3, JULY 2014.

[3] Heng Nian, Member, IEEE, Peng Cheng, and Z. Q. Zhu, Fellow, IEEE," Independent Operation of DFIG-Based WECS Using Resonant Feedback Compensators Under Unbalanced Grid Voltage Conditions" IEEE Trans. On Power Electronics, VOL. 30, NO. 7, JULY 2015.

[4] I. M. Mehedi, N. Saad, M. A. Magzoub, U. M. Al-Saggaf and A. H. Milyani, "Simulation Analysis and Experimental Evaluation of Improved Field-Oriented Controlled Induction Motors Incorporating Intelligent Controllers," in IEEE Access, vol. 10, pp. 18380-18394, 2022.

[5] M. Abolhassani, P. Niazi, H. Tolivat, and P. Enjeti, "A sensorless Integrated Doubly-Fed Electric Alternator/Active filter (IDEA) for variable speed wind energy system," in Conf. Rec. 38th IEEE IAS Annu. Meeting, 2003, pp. 507–514.

[6] R. Datta and V. T. Ranganathan, "A simple positionsensorless algorithm for rotor-side field-oriented control of wound-rotor induction machine,"IEEE Trans. Ind. Electron., vol. 48, no. 4, pp. 786–793, Aug. 2001.

[7] L. Morel, H. Godfroid, A. Mirzaian, and J. M. Kauffmann, "Doublefed induction machine: Converter optimisation and field oriented control without position sensor," Proc. Inst. Elect. Eng.—Elect. Power Appl., vol. 145, no. 4, pp. 360–368, Jul. 1998.

[8] E. Bogalecka and Z. Krzeminski, "Sensorless control of a double-fed machine for wind power generators," in Proc. EPE-PMC, Dubrovnik and Cavtat, Croatia, 2002, [CD-ROM].

[9] B. Hopfensperger, D. J. Atkinson, and R. A. Lakin, "Stator-flux-oriented control of a doubly-fed induction machine with and without position encoder," Proc. Inst. Elect. Eng.—Elect. Power Appl., vol. 147, no. 4, pp. 241–250, Jul. 2000.

[10] O. A. Mohammed, Z. Liu, and S. Liu, "A novel sensorless control strategy of doubly fed induction motor and its examination with the physical modeling of machines," IEEE Trans. Magn., vol. 41, no. 5, pp. 1852–1855, May 2005.

[11] L. Xu and W. Cheng, "Torque and reactive power control of a doubly fed induction machine by position sensorless scheme," IEEE Trans. Ind.Appl., vol. 31, no. 3, pp. 636–642, May/Jun. 1995.

[12] P. Naganathan and S. Srinivas, "MTPA Associated DTC Methodologies for Enhanced Performance and Energy Savings in Electric Vehicle Mobility With Induction Motor Drive," in IEEE Transactions on TransportationElectrification, vol. 8, no. 2, pp. 1853-1862, June 2022.

[13] R. Ghosn, C. Asmar, M Pietrzak-David, and B. De Fornel, "A MRASsensorless speed control of doubly fed induction machine," in Proc. Int.Conf. Elect. Mach., 2002, pp. 26–28.

[14] R. Ghosn, C. Asmar, M. Pietrzak-David, and

B. De Fornel, “A MRAS Luenberger sensorless speed control of doubly fed induction machine,” in Proc. Eur. Power Electron. Conf., 2003, [CD-ROM].

[15] R. Cardenas, R. Pena, J. Proboste, G. Asher, and J. Clare, “MRAS observer for sensorless control of standalone doubly fed induction generators,”IEEE Trans. Energy Convers., vol. 20, no. 4, pp. 710–718,Dec. 2005.

[16] R. Peña, R. Cardenas, J. Proboste, G. Asher, and J. Clare, “Sensorless control of doubly-fed induction generators using a rotor-current-based MRAS observer,” IEEE Trans. Ind. Electron., vol. 55, no. 1, pp. 330–339, Jan.2008.

[17] R. Pena, R. Cardenas, J. Proboste, G. Asher, and J. Clare, “Sensorless control of a slip ring induction generator based on rotor current MRAS observer,” in Proc. 36th IEEE PESC, 2005, pp. 2508–2513.

[18] M. S. Carmeli, M. Iacchetti, and R. Perini, “A MRAS observer applied to sensorless doubly fed induction machine drives,” in Proc. IEEE ISIE,2010, vol. 1, pp.3077–3082.

[19] L. Mohan, K. Pant and P. P. Rajeevan, "A Speed Range Extension Scheme for Scalar-Controlled Open-End Winding Induction Motor Drives," in IEEE Transactions on Industry Applications, vol. 58, no. 2, pp. 2055-2062, March-April 2022.

[20] B. Mwinyiwiwa, Y. Zhang, B. Shen, and B.-T. Ooi, “Rotor position phase-locked loop for decoupled P–Q control of DFIG for wind powergeneration,” IEEE Trans.Energy Convers., vol. 24, no. 3, pp. 758-756,Sep 2009.

[21] K. Gogas, G. Joos, B. T. Ooi, Y. Z. Zhang, and B.Mwinyiwiwa, “Designof a robust speed and position sensorless decoupled P-Q controlled doubly-fed induction generator for variable-speed wind energy applications,”inProc. IEEE Canada EPC, 2007, pp. 62–67.

[22] R. Cárdenas, R. Peña, S. Alepuz, and G. Asher, “Overview of Control Systems for the Operation of DFIGs in Wind Energy Applications” IEEE Trans. Ind.Elec., vol. 60, no. 7, july,2013.

[23] Etienne Tremblay, Sergio Atayde, and Ambrish Chandra, ”Comparative Study of Control Strategies for the Doubly Fed Induction Generator in Wind Energy Conversion Systems: A DSP-Based Implementation Approach “IEEE TRANSACTIONS ON SUSTAINABLE ENERGY,2011.